Physics Letters B 841 (2023) 137933

Contents lists available at ScienceDirect

Physics Letters B

journal homepage: www.elsevier.com/locate/physletb

Axial and triaxial degrees of freedom in ^{72}Zn

S. Hellgartner [a], D. Mücher [b,c,d,*], K. Wimmer [e,f,g,*], V. Bildstein [c], J.L. Egido [i], R. Gernhäuser [a], R. Krücken [h], A.K. Nowak [a], M. Zielińska [j], C. Bauer [k], M.L.L. Benito [l], S. Bottoni [m,n], H. De Witte [n], J. Elseviers [n], D. Fedorov [l], F. Flavigny [o], A. Illana [f,r], M. Klintefjord [p], T. Kröll [k], R. Lutter [q], B. Marsh [l], R. Orlandi [f], J. Pakarinen [r], R. Raabe [n], E. Rapisarda [n,l,s], S. Reichert [a], P. Reiter [b], M. Scheck [t], M. Seidlitz [b], B. Siebeck [b], E. Siesling [l], T. Steinbach [b], T. Stora [l], M. Vermeulen [u], D. Voulot [l], N. Warr [b], F.J.C. Wenander [l]

[a] Physik-Department, Technische Universität München, 85748 Garching, Germany
[b] Institut für Kernphysik, Universität zu Köln, 50937 Köln, Germany
[c] College of Physics & Engineering Science, University of Guelph, 50 Stone Road East Guelph, Ontario N1G 2W1, Canada
[d] Physical Sciences Division, TRIUMF, Vancouver, British Columbia, V6T 2A3, Canada
[e] GSI Helmholtzzentrum für Schwerionenforschung, D-64291 Darmstadt, Germany
[f] Instituto de Estructura de la Materia, CSIC, E-28006 Madrid, Spain
[g] Department of Physics, The University of Tokyo, Hongo, Bunkyo-ku, Tokyo 113-0033, Japan
[h] Nuclear Science Division, Lawrence Berkeley National Laboratory, Berkeley, CA 94720, USA
[i] Departamento de Física Teórica, Universidad Autónoma de Madrid, E-28049 Madrid, Spain
[j] IRFU, CEA, Université Paris-Saclay, 91191 Gif-sur-Yvette, France
[k] Institut für Kernphysik, Technische Universität Darmstadt, Germany
[l] ISOLDE, CERN, CH-1211, Geneva, Switzerland
[m] Dipartimento di Fisica, Università degli Studi di Milano and INFN Sez. Milano, Milano I-20133, Italy
[n] KU Leuven, Instituut voor Kern- en Stralingsfysica, 3001 Leuven, Belgium
[o] Normandie Univ, ENSICAEN, UNICAEN, CNRS/IN2P3, LPC Caen, 14000 Caen, France
[p] Department of Physics, University of Oslo, N-0316 Oslo, Norway
[q] Department of Physics, Ludwig Maximilian Universität München, 85748 Garching, Germany
[r] Department of Physics, University of Jyväskylä, P.O. Box 35, FI-40014 Jyväskylä, Finland
[s] Paul Scherrer Institut, Villigen, Switzerland
[t] School of Computing, Engineering, and Physical Sciences, University of the West of Scotland, Paisley PA1 2BE, UK
[u] Department of Physics, University of York, YO10 5DD, United Kingdom

ARTICLE INFO

Article history:
Received 22 June 2021
Received in revised form 24 March 2023
Accepted 21 April 2023
Available online 26 April 2023
Editor: B. Blank

Keywords:
Multiple Coulomb excitation
^{72}Zn
$N = 40$ sub-shell closure
Triaxiality

ABSTRACT

The unstable $N = 42$ nucleus ^{72}Zn has been studied using multiple safe Coulomb excitation in inverse kinematics. The experiment was performed at the REX-ISOLDE facility at CERN making first use of the silicon detector array C-REX in combination with the γ-ray spectrometer Miniball. The high angular coverage of C-REX allowed to determine the reduced transition strengths for the decay of the yrast 0_1^+, 2_1^+ and 4_1^+ as well as of the 0_2^+ and 2_2^+ states in ^{72}Zn. The quadrupole moments of the 2_1^+, 4_1^+ and 2_2^+ states were extracted. Using model independent quadrupole invariants, the ground state of ^{72}Zn was found to have an average deformation in the γ degree of freedom close to maximum triaxiality. In comparison to experimental data in zinc isotopes with $N < 40$, the collectivity of the 4_1^+ state in neutron-rich ^{72}Zn is significantly larger, indicating a collective yrast band based on the ground state of ^{72}Zn. In contrast, a low experimental $B(E2; 0_2^+ \rightarrow 2_1^+)$ strength was determined, indicating a different structure for the 0_2^+ state. Shell-model calculations propose a 0_2^+ state featuring a larger fraction of the (spherical) $N = 40$ closed-shell configuration in its wave function than for the 0_1^+ ground state.

The results were also compared with beyond mean field calculations which corroborate the large deformation in the γ degree of freedom, while pointing to a more deformed 0_2^+ state. These experimental and theoretical findings establish the importance of the γ degree of freedom in the ground state of ^{72}Zn,

* Corresponding authors.
E-mail addresses: muecher@ikp.uni-koeln.de (D. Mücher), k.wimmer@gsi.de (K. Wimmer).

https://doi.org/10.1016/j.physletb.2023.137933

located between the ^{68,70}Ni nuclei that have spherical ground states, and ^{76}Ge, which has a rigid triaxial shape.

One of the fundamental properties of the atomic nucleus is its shape. Nuclei with a closed-shell configuration are spherical, while deformation can arise from quadrupole correlations in open-shell nuclei. The collective, or Bohr Hamiltonian [1] describes the dynamics of nuclei in terms of the deformation parameters β and γ. The quantity β measures the axial-symmetric deformation of an ellipsoid, while γ relates to the deviation from axial symmetry.

Two approximations of the Bohr Hamiltonian are often used when discussing the γ degree of deformation: the triaxial γ-rigid rotor of the Davydov-Filippov model [2], and the γ independent (or γ unstable) Wilets-Jean model [3].

A transitional region is observed close to the harmonic oscillator shell gap $N = 40$. The magic Ni isotopic chain at $Z = 28$ exhibits spherical ground states across $N = 40$. Adding four protons leads to more deformed Ge isotopes at $Z = 32$; Ge isotopes were found to undergo a transition from γ-soft in ^{72}Ge [4] to γ-rigid in ^{76}Ge. ^{76}Ge is one of the few cases where rigid triaxiality in low-lying states has been observed through the staggering of states in the γ band [5] and from electromagnetic matrix elements [6].

Indication for changes in deformation can already be found for the $Z = 30$ chain of Zn isotopes. Coulomb excitation and lifetime measurements [7–11] find increased $B(E2; 2_1^+ \rightarrow 0_{gs}^+)$ values in ^{72,74}Zn compared to the Zn isotopes below $N = 40$ indicating the onset of deformation, but these earlier experiments were not sensitive to the γ degree of deformation. For ^{72}Zn, the g-factor of the 2_1^+ state, which is close to the hydro-dynamical limit, indicates deformation [12] and triaxiality was suggested to be present in ^{73}Zn based on the observation of a deformed $5/2^+$ isomeric state [13]. This onset of deformation and triaxiality in Zn is supported by beyond mean field calculations. Calculations employing the symmetry conserving configuration mixing approach [14] presented in Ref. [12], as well as the five-dimensional collective quadrupole Hamiltonian (5DCH) treatment [15] predict significant triaxial deformation of the ground states of $^{70-74}$Zn. Large-scale Monte-Carlo shell-model calculations predict triaxiality for $^{72-74}$Zn, but do not find triaxial shapes for the ground states of ^{71,75}Zn [13]. A recent experimental study of the ^{66}Zn nucleus also highlights the importance of the triaxial degree of freedom before $N = 40$ and suggests large fluctuations of the wave functions around $\gamma \approx 30°$ [16].

Nuclei in this region around neutron number $N = 40$ also show interesting occurrences of shape coexistence [17]. In ^{70}Ni, triple shape coexistence of a spherical ground state with prolate and oblate deformed excited 0^+ states is predicted by Monte-Carlo shell-model calculations [18]. Experimentally, a candidate for an excited 0^+ state has been observed at 1567 keV [19]. In ^{72}Ge, the first excited state is a 0^+ state and has been classified as an intruder state of spherical nature [4], while the ground state is deformed.

In this letter, we study the unstable $Z = 30$ isotope ^{72}Zn at $N = 42$ via multi-step safe Coulomb excitation. This method is sensitive to the reduced transition probabilities and the spectroscopic quadrupole moments. Furthermore, the data set also allows the extraction of approximate shape invariants, which give access to the shape of the nucleus in a model independent way. This way, we test triaxiality in the direct vicinity of the "doubly magic" ^{68}Ni nucleus and gain new insight into the coexisting shapes in this region.

The experiment was performed at the REX-ISOLDE facility at CERN [20,21]. The radioactive ^{72}Zn beam was produced by the 1.4 GeV proton beam of the PS booster impinging on a UC_x ISOL production target. To select the ^{72}Zn atoms from other reaction products from the primary target, they were laser ionized at the Resonant Ionization Laser Ion Source [22], accelerated to 30 keV, and mass separated in the High Resolution Separator. The singly-charged ^{72}Zn ions were bunched in the penning trap REX-TRAP and bred to a higher charge state, $Q = 20$, in the REX-EBIS. Finally, the ^{72}Zn ions were accelerated to beam energies of $E_{beam} = 2.85$ MeV/nucleon in the normal-conducting linear accelerator REX. The average beam intensity of ^{72}Zn was $3.5(3) \cdot 10^7$ ions/s. A small fraction of surface-ionized ^{72}Ga was transmitted as well. The isobaric contamination, 6.9(6)% of the total beam, was determined using a modified laser on/off method. The post-accelerated beam impinged on a 1.17 mg/cm^2 thick ^{109}Ag target located in the center of the C-REX array [23] and surrounded by 8 six-fold segmented high-purity Ge triple cluster detectors of the Miniball array [24] used for high resolution spectroscopy of the γ radiation emitted by the Coulomb excited nuclei. The silicon detector array C-REX was designed and first used for this experiment, allowing for the selection of projectile and target-like reaction products with a large angular coverage. The design of C-REX is based on the transfer reaction setup T-REX [25] featuring the same scattering chamber and type of detectors, but it is optimized for Coulomb-excitation experiments. In particular, it offers a good coverage of large center-of-mass scattering angles for normal-kinematics experiments, increasing the experimental sensitivity to multi-step processes in Coulomb excitation. C-REX features two annular double-sided silicon strip detectors (DSSSD) covering laboratory angles $\theta_{lab} = [21.0° - 60.2°]$ and $[153° - 172°]$. Each detector is divided into four quadrants with 16 annular rings ($\Delta r =$ 2 mm) and 24 radial strips ($\Delta\phi = 3.4°$), each. In addition to the DSSSDs, C-REX is equipped with four squared single sided silicon strip detectors ($\theta_{lab} = [102° - 153°]$) which are arranged in a box. Their 16 resistive strips feature a pitch of $\Delta d = 3.125$ mm each and are orientated perpendicular to the beam axis. The electronics of C-REX is identical to the T-REX one and allows for high particle count rates and particle-particle coincidences. For this, in contrast to T-REX, the trigger signals were generated for each of the quadrants independently. More details can be found in Ref. [23].

The high beam intensity, in combination with the large angular coverage of the C-REX array, allows the study of multi-step Coulomb excitation of ^{72}Zn with high precision. Since the γ rays originating from the de-excitation of the ejectile and recoil nuclei are emitted in flight, a good Doppler correction is essential. Fig. 1 shows a γ-ray energy spectrum coincident with ^{72}Zn particles detected in the forward part of C-REX. The main peaks in Fig. 1 are the yrast $2_1^+ \rightarrow 0_{gs}^+$ ($E_\gamma = 653$ keV) and $4_1^+ \rightarrow 2_1^+$ ($E_\gamma = 847$ keV) transitions as well as the decay of the 2_2^+ state to the ground ($E_\gamma = 1658$ keV) and 2_1^+ states ($E_\gamma = 1004$ keV). The level scheme with the observed transitions is shown in Fig. 4. The decays of excited states in the ^{109}Ag target nucleus are observed as broad peaks when the Doppler correction assumes the Zn trajectory. A small peak at 166 keV is associated with the ^{72}Ga beam contamination. When gating on ^{72}Zn ions that are scattered to laboratory backward angles, the 858-keV $0_2^+ \rightarrow 2_1^+$ transition is clearly identified (see inset of Fig. 1), indicating that this state is mostly populated by multi-step excitation with growing differential cross sections for larger $\theta_{c.m.}$ angles. With the available beam intensities, the 0_2^+ state could therefore only be studied with the newly de-

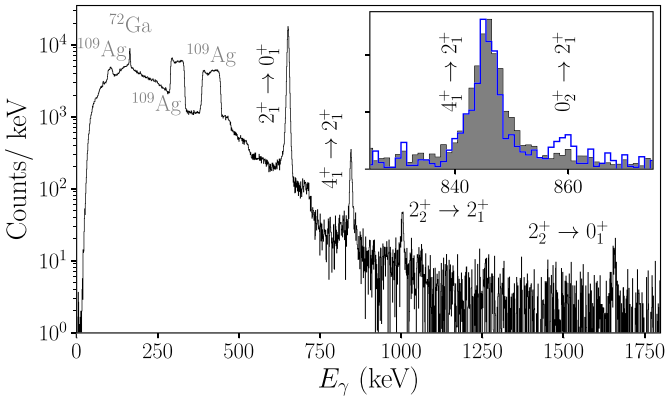

Fig. 1. Doppler corrected and background subtracted γ-ray energy spectrum measured in coincidence with ^{72}Zn ions detected in the forward C-REX detectors. The Doppler correction has been performed assuming the γ rays are emitted from the ^{72}Zn. Known transitions in ^{72}Zn are indicated. Indicated in gray are contributions from the strongest ^{109}Ag γ-ray transitions as well as from the isobaric beam contaminant ^{72}Ga. The inset shows a comparison of the Doppler corrected γ-ray spectrum of the forward (gray, filled) and backward (blue) C-REX detectors. In backward direction, additionally the $0_2^+ \to 2_1^+$ transition of ^{72}Zn at $E_\gamma = 858$ keV is present.

veloped C-REX array covering large scattering angles and not with the previous setup at REX-ISOLDE [24].

In Coulomb excitation [26] the excitation cross section for final states J_f depends not only on the transitional $E2$ matrix elements for the direct excitation, $\langle 0_{gs}^+ || E2 || J_f \rangle$, and second order effects from multi-step excitations through intermediate states, $\langle 0_{gs}^+ || E2 || J_i \rangle \langle J_i || E2 || J_f \rangle$, but also on the diagonal matrix elements (quadrupole moments Q) and their signs. In contrast to previous lifetime measurements and Coulomb excitation at intermediate beam energies the excellent statistics of the present experiment and the high angular coverage of the new C-REX detector allow to analyze the angular distributions of the Coulomb-excitation cross sections and determine the matrix elements. The matrix elements and their respective signs were obtained by fitting the detected γ-ray yields with a multi-step Coulomb-excitation calculation obtained with the CLX [27,28] and GOSIA [29] codes. To avoid systematic uncertainties introduced by an evaluation of absolute luminosity and detection efficiencies, a relative measurement is performed, i.e. the yields are normalized using a γ-ray transition with a known (partial) lifetime. In the present work, a set of 26 electric and magnetic matrix elements of ^{109}Ag was used for the normalization [23]. For this, the data for the γ-ray yields for ^{109}Ag were divided into 14 angular bins to obtain in total 110 γ-ray yield data points used in the fit. The data for the γ-ray yields for ^{72}Zn were divided into the same angular bins. Since the yield could not be determined in every bin for each of the five observed transitions, bins have been combined and a total of 45 γ-ray yield data points were used in the global minimization procedure for ^{72}Zn. In addition, upper limits, for example for the observation of the $6^+ \to 4^+$ transition, have been introduced. The matrix elements for ^{72}Zn have then been obtained following the GOSIA-GOSIA2 procedure described in Ref. [30]. The strong sensitivity of the data to the spectroscopic quadrupole moments (diagonal matrix elements) is shown for the $2_{1,2}^+$ and 4_1^+ states in Fig. 2 and the results of the minimization are listed in Table 1. As a cross check, additionally the measured lifetime of the 2_1^+ state of ^{72}Zn [9–11] has been used for normalization, which results in a consistent set of matrix elements. The results for the $B(E2)$ values of the $2_1^+ \to 0_1^+$ and $4_1^+ \to 2_1^+$ transitions in ^{72}Zn are shown in Fig. 3 and compared with the neighboring Zn isotopes and previous experimental results.

The $B(E2; 2_1^+ \to 0_1^+)$ value agrees very well with previous Coulomb-excitation and lifetime measurements [7,9–11]. However, the measured $B(E2; 4_1^+ \to 2_1^+)$ values indicate larger values than deduced from lifetime measurements. For $N = 42$ and 44, Coulomb-excitation experiments, including the present study, yield higher $B(E2)$ values compared to lifetime measurements of Refs. [10,11,37]. Indirect feeding through transitions from higher-lying states can result in systematically too large lifetimes extracted in those experiments. This effect was investigated in Ref. [10] by gating on the excitation energy in the reaction residue.

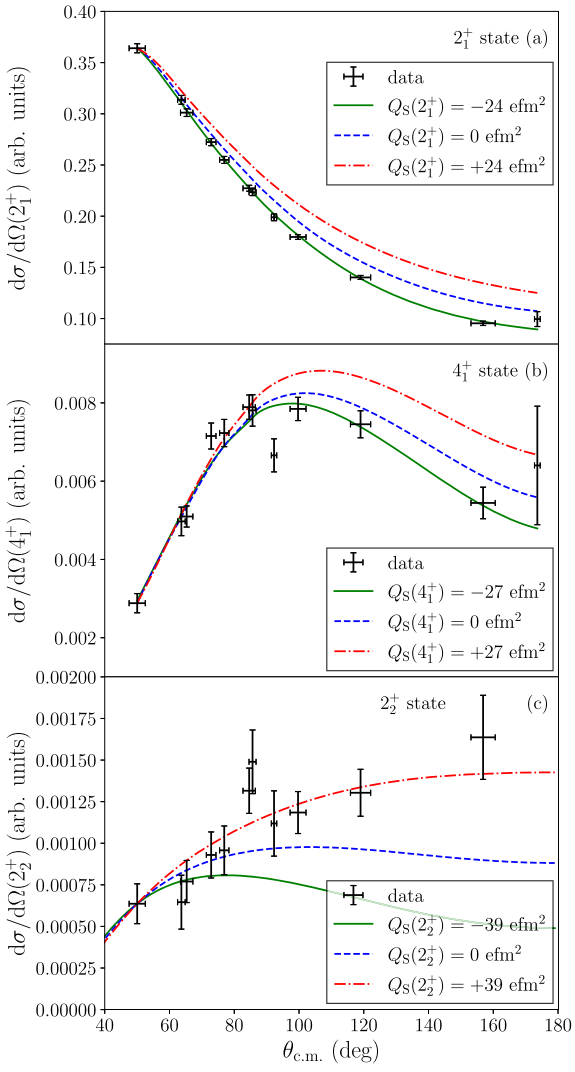

Fig. 2. Differential cross section for the excitation of the 2_1^+ (top), 4_1^+ (middle) and 2_2^+ (bottom) states. The data, divided into the 14 angular ranges are shown in black and for the horizontal error bars it has been assumed that the counts are uniformly distributed in that angular bin. The green (solid) curve shows the calculated angular distribution using the best fit values for the transitional and diagonal matrix elements. For comparison, also calculations using $Q_S = 0$ (blue, dashed) or a positive quadrupole moment (red, dashed-dotted) are shown. In these cases the transitional matrix element has been adjusted to the data point at $\theta_{c.m.} = 50°$.

The present experimental data also allowed to determine the diagonal matrix elements. Both the 2_1^+ and the 4_1^+ have negative spectroscopic quadrupole moments, while the value obtained for the 2_2^+ state is positive (see Fig. 2). The data also allowed to deduce the $E2/M1$ mixing ratio for the $2_2^+ \to 2_1^+$ transition with a negligible $M1$ contribution [23]. The influence of the $\langle 6_1^+ || E2 || 4_1^+ \rangle$ matrix element on the results has been investigated. Using the conservative upper limit for the observation of the $6_1^+ \to 4_1^+$ transition from the present data or the lifetime measured in Ref. [11] results in negligible changes of the deduced $\langle 4_1^+ || E2 || 2_1^+ \rangle$ matrix element.

Table 1
Transition energies, matrix elements, reduced transitions strengths $B(\pi\lambda)$, and quadrupole moments for states and transitions in ^{72}Zn determined from the GOSIA-GOSIA2 analysis. The uncertainties are listed separately for statistical and systematic contributions. The statistical uncertainties include the uncertainties of the normalization as well as the statistical errors of the count rates in the individual peaks. In addition, a systematic uncertainty of 5% is added to the matrix elements to account for the approximations used in the GOSIA code [29,30]. Theoretical results based on shell-model calculations with the jj44c and JUN45 effective interactions and mean-field generator coordinate method (GCM) calculations are also presented.

	Experiment			SM jj44c		SM JUN45		Triaxial GCM	
Transition	E_γ (keV)	$\langle J_i\|\|E2\|\|J_f\rangle$ (eb)	$B(E2)$ (e^2 fm^4)	E_γ (keV)	$B(E2)$ (e^2 fm^4)	E_γ (keV)	$B(E2)$ (e^2 fm^4)	E_γ (keV)	$B(E2)$ (e^2 fm^4)
$2_1^+ \to 0_1^+$	653	$0.424^{+0.002}_{-0.002} \pm 0.021$	$360^{+3}_{-3} \pm 36$	818	384.4	1007	315.0	789	547.8
$2_2^+ \to 0_1^+$	1658	$0.074^{+0.005}_{-0.004} \pm 0.004$	$11.0^{+1.4}_{-1.1} \pm 1.1$	1929	3.9	1906	2.9	2043	37.0
$2_2^+ \to 2_1^+$	1004	$0.32^{+0.01}_{-0.01} \pm 0.02$	$205^{+12}_{-17} \pm 21$	1111	326.3	899	421.2	1254	385.0
$4_1^+ \to 2_1^+$	847	$0.68^{+0.01}_{-0.01} \pm 0.03$	$514^{+9}_{-9} \pm 52$	861	508.6	954	327.6	1182	817.2
$0_2^+ \to 2_1^+$	858	$0.14^{+0.01}_{-0.03} \pm 0.01$	$196^{+33}_{-73} \pm 20$	1009	93.8	769	126.4	1591	260.0
Transition	E_γ (keV)	$\langle J_i\|\|M1\|\|J_f\rangle$ (μ_N)	$B(M1)$ (10^{-4} μ_N^2)	E_γ (keV)	$B(M1)$ (10^{-4} μ_N^2)	E_γ (keV)	$B(M1)$ (10^{-4} μ_N^2)	E_γ (keV)	$B(M1)$ (10^{-4} μ_N^2)
$2_2^+ \to 2_1^+$	1004	$-0.06^{+0.07}_{-0.03} \pm 0.001$	$7.2^{+16.8}_{-7.2} \pm 0.1$	1111	372	899	2202	1254	3.73
State	E (keV)	$\langle J_i\|\|E2\|\|J_i\rangle$ (eb)	Q_S (efm^2)	E (keV)	Q_S (efm^2)	E (keV)	Q_S (efm^2)	E (keV)	Q_S (efm^2)
2_1^+	653	$-0.31^{+0.04}_{-0.04} \pm 0.01$	$-24^{+3}_{-3} \pm 1$	818	−27.5	1007	−4.7	789	-38.5
4_1^+	1500	$-0.36^{+0.06}_{-0.10} \pm 0.02$	$-27^{+5}_{-7} \pm 1$	1679	−45.3	1961	−41.2	1971	-49.9
0_2^+	1511			1828		1776		2380	
2_2^+	1658	$+0.52^{+0.05}_{-0.03} \pm 0.03$	$+39^{+4}_{-3} \pm 2$	1929	+17.7	1906	+3.8	2043	+38.4

Compared to the less neutron-rich isotopes, a significant increase is observed in the $B(E2; 2_1^+ \to 0_1^+)$ and $B(E2; 4_1^+ \to 2_1^+)$ values for $N = 42$ compared to $^{64-70}$Zn. For the $B(E2; 4_1^+ \to 2_1^+)$ value the data for the nucleus ^{70}Zn at $N = 40$ remain conflicting. Such an increase in deformation is in agreement with the reduction of the excitation energies of the 2_1^+ and 4_1^+ states by adding four neutrons to ^{68}Zn. The increase in collectivity at and beyond $N = 42$ is in also agreement with earlier observations for the Zn nuclei [9] and the evolution along the Ni isotopic chain.

The present results are compared to shell-model calculations in the jj44 model space ($1f_{5/2}$, $2p_{3/2}$, $2p_{1/2}$ and $1g_{9/2}$ for both protons and neutrons) using the jj44c [34,35] and JUN45 [36] residual interactions. The calculations have been performed with the KSHELL code [38]. In all shell-model calculations, effective charges determined for this model space, $(e_p, e_n) = (1.5, 1.1)$, and g-factors, $g_s^{\text{eff}} = 0.7 g_s^{\text{free}}$ [36,39], were used when calculating transition probabilities. For the harmonic oscillator potential employed to calculate the transition rates, we used $\hbar\omega = 41A^{-1/3}$. The results are presented in Table 1 and Figs. 3 and 4. The calculations all reproduce the excitation energies as well as the magnitude and trend of the $B(E2)$ values well. The rather steep increase in $B(E2; 2_1^+ \to 0_1^+)$ values from ^{68}Zn to ^{72}Zn is better described using the jj44c interaction. Experimentally, we observe a similar increase for the $B(E2; 4_1^+ \to 2_1^+)$ strength which is not fully reflected in any of our calculations, but a kink is observed at $N = 38$ using the jj44c interaction. Overall, the two interactions produce rather similar results.

Looking now into the wave function composition of states, for ^{72}Zn the majority of neutron configurations for the $0_1^+, 2_1^+$, and 4_1^+ states have two neutrons excited from the $\nu 0f_{5/2}$, $1p_{1/2}$, or $1p_{3/2}$ orbitals to the $0g_{9/2}$ orbital above $N = 40$. This scattering of neutron pairs above the $N = 40$ harmonic oscillator gap can be understood as an effect arising from polarization of the $Z = 28$ core [40,41]. Note that all interactions used here reflect the core polarization only indirectly through their fitted effective matrix elements and effective charges. Our calculations are consistent with the assumption that core polarization and increased $\nu 0g_{9/2}$ occupation play a vital role in the increased $B(E2)$ values and lowering of excitation energies in the ground state band beyond $N = 38$. The experimental results clearly indicate an enhanced $B(E2; 4_1^+ \to 2_1^+)$ strength beyond $N = 40$. These results will serve future more sophisticated calculations as bench mark.

It is now interesting to study the shape and the nature of the deformation of ^{72}Zn. As shown in Fig. 4 the 4_1^+, 2_2^+, and 0_2^+ states lie close in energy as expected in a vibrational model, where the two-phonon excitations are located at twice the energy of the one-phonon 2_1^+ state. However, for $J_i = 4_1^+, 2_2^+, 0_2^+$ a constant ratio $B(E2; J_i \to 2_1^+)/B(E2; 2_1^+ \to 0_1^+) = 2$ would be expected in the vibrational model, while this is clearly not experimentally observed.

On the other hand, the ^{72}Zn nucleus can also not be described assuming a rigid axial deformation, in which case the quadrupole moment is related to the $B(E2)$ value

$$|Q_S(2_1^+)| = \frac{2}{7}\sqrt{16\pi B(E2; 2_1^+ \to 0_1^+)}. \quad (1)$$

For the present case, this yields $|Q_S(2_1^+)| = 38.4(19)$ efm^2, significantly larger than determined from the present Coulomb-excitation measurement, suggesting that triaxiality plays a major role in ^{72}Zn.

It is therefore intriguing to compare ^{72}Zn to the geometric triaxial Davydov-Filippov model [2]. The ratios of the excitation energies of the 2_2^+ and 4_1^+ states to the one of the first excited 2_1^+ state as well as the $B(E2; 2_2^+ \to 0_1^+)/B(E2; 2_1^+ \to 0_1^+)$ and $B(E2; 2_2^+ \to 2_1^+)/B(E2; 2_1^+ \to 0_1^+)$ ratios are well reproduced by assuming a static triaxial deformation with $\gamma = 22 - 25°$. It is, however, impossible to experimentally distinguish between γ-soft and γ-rigid deformation based on these arguments. Previous experimental and theoretical studies [9] of ^{72}Zn suggested γ-softness for ^{72}Zn based on the energy ratio $R_{22} = E(2_\gamma^+)/E(2_1^+) = 2.54$ close to the value 2.5 expected in the γ-soft Wilets-Jean model [3]. Although a tentative assignment for the 3^+ and 4^+ states belonging to the γ band in ^{72}Zn [9] points towards γ-softness rather than γ-rigid deformation, the γ band in ^{72}Zn is experimentally not established.

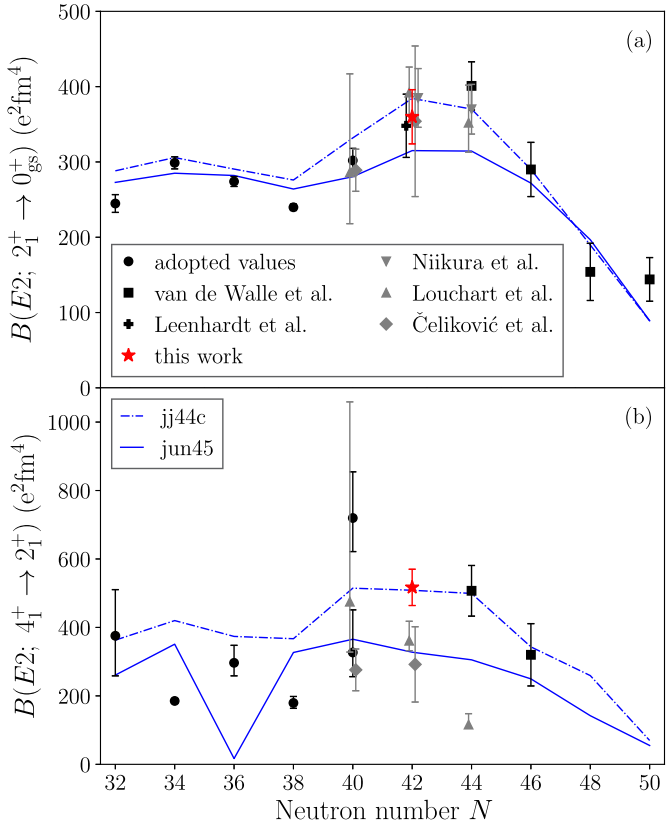

Fig. 3. Comparison of the $B(E2)$ values for the $2_1^+ \rightarrow 0_1^+$ (a) and $4_1^+ \rightarrow 2_1^+$ (b) transitions with previous measurements. Adopted values [31,32] are shown as black circles. Previous Coulomb-excitation studies at REX-ISOLDE [8] and GANIL [7] are labeled with black squares and crosses, respectively. Gray triangles and circles represent the results from lifetime measurements [9–11]. The results of the present study are highlighted as red stars. Note that for the $4_1^+ \rightarrow 2_1^+$ transition of ^{70}Zn, the adopted value is the weighted average of the lifetime measurements of Refs. [10,11], while an older value is much higher, but potentially the transition is contaminated by the $3_1^- \rightarrow 2_1^+$ transition of the same energy [32,33]. The solid and dotted-dashed lines show the results of shell-model calculations using the jj44c and JUN45 effective interactions [34–36].

A model independent measure of the nuclear shape can be obtained from rotationally invariant zero-coupled products [42,43]. The deformation is expressed in terms of the two parameters Q and δ. For a certain state s, expanding all intermediate states i,

$$\langle Q^2 \rangle = \sqrt{\frac{5}{2I_s+1}} \sum_i \langle s||E2||i\rangle\langle i||E2||s\rangle \begin{Bmatrix} 2 & 2 & 0 \\ I_s & I_s & I_i \end{Bmatrix} \quad (2)$$

yields the quadrupole invariant Q^2, which is related to the deformation β by

$$\langle Q^2 \rangle = \left(\frac{3}{4\pi} Z R_0^3\right)^2 \langle \beta^2 \rangle \quad (3)$$

with $R_0 = r_0 A^{1/3}$. The asymmetry, related to the parameter γ in the Bohr Hamiltonian, is described by $\langle cos3\delta \rangle$, and can be obtained by summation over all combinations of intermediate states i and j

$$\langle Q^3 cos3\delta \rangle = -\sqrt{\frac{35}{2}} \frac{1}{2I_s+1} \times$$
$$\sum_{i,j} \langle s||E2||i\rangle\langle i||E2||j\rangle\langle j||E2||s\rangle \begin{Bmatrix} 2 & 2 & 2 \\ I_s & I_j & I_i \end{Bmatrix}. \quad (4)$$

The angle δ can then be obtained by assuming $\langle Q^3 cos3\delta \rangle \approx \langle Q^2 \rangle^{3/2} \langle cos3\delta \rangle$. Summing over the experimentally observed states and the extracted matrix elements these quantities amount to $\langle Q^2 \rangle = 0.185(18)$ e^{2}b^2 and $\langle \cos 3\delta \rangle = 0.34(10)$ for the 0_1^+ ground state. Using Eq. (3) and associating δ with the Bohr parameter γ, these yield $\beta = 0.241(12)$ and $\gamma = 23.3(21)°$. This suggests that ^{72}Zn is moderately deformed and shows a significant deformation in the γ degree of freedom. Obviously, the sums in Eqs. (2) and (4) are truncated and include only experimentally measured matrix elements. The results should therefore be regarded as an approximation [44]. It would be interesting to determine the variance of $\langle Q^2 \rangle$ and $\langle cos3\delta \rangle$ to determine the rigidity in the deformation and triaxiality directions and gauge if ^{72}Zn is γ-soft or rigid in nature. However, the statistics of the present study is not sufficient for this analysis.

The method of extracting the quadrupole invariants can also be applied to the shell-model calculations. Including up to 200 states in the calculation, these yield $\langle Q\,(0_1^+)^2 \rangle = 0.203(69)$ and 0.166(70) for the jj44c and JUN45 effective interactions, respectively, while the triaxiality parameters amount to $\langle cos3\delta \rangle = 0.45(45)$ and 0.30(50), where the values in parentheses give the variance of the deformation parameters. This suggests a larger degree of triaxiality in the JUN45 calculations, and points to the fact that the small calculated quadrupole moment for the 2_1^+ state shown in Table 1 is resulting from the superposition of oblate and prolate configurations in a γ-soft nucleus. The calculated values $\beta = 0.252(87)$ and $\beta = 0.228(99)$ for jj44c and JUN45 are in good agreement with experiment, as are the values $\gamma = 21(22)°$ and $\gamma = 24(22)°$, respectively. The 5DCH calculations of Ref. [15] give $\beta = 0.239(80)$ and $\gamma = 26(13)°$.

The obtained set of $E2$ matrix elements was not sufficient to obtain quadrupole invariants for the 0_2^+ state. It is, however, clear that the 0_2^+ state is of different nature than the ground state, as indicated by the much weaker transition to the 2_1^+ state, compared to the $0_1^+ \rightarrow 2_1^+$ one. The structural difference can be further explored by looking at the calculated wave function composition of the 0^+ states. In all our calculations, the ground state has dominant wave function contributions where two neutrons from the $0f_{5/2}$, $1p_{1/2}$, or $1p_{3/2}$ orbitals are excited above the $N = 40$ subshell gap to the $0g_{9/2}$ level. The excited 0_2^+ state on the other hand is dominated by closed-shell configurations with only two neutrons in the $0g_{9/2}$ level.

In order to get more insights, we have also performed Generator Coordinate Method (GCM) calculations with the deformation parameters (β, γ) as coordinates and exact particle number and angular momentum projection (PNAMP) [14]. In the calculations, the Gogny force with the D1S parametrization was used. In Fig. 5 a), we display the potential energy surface in the PNAMP approach, i.e., without mixing of the different (β, γ) values, for $J = 0\,\hbar$. A broad triaxial minimum has an expectation value of $\beta = 0.32(2)$ with $\gamma = 22(331)°$. Again, values in parentheses show the variance of the expectation values. The surface is rather soft in γ and very steep for larger β values, except along the prolate axis, where it shows a rather soft behavior. In panel b), we display the collective wave function of the ground state. The wave function is very extended at a deformation that is somewhat larger than the energy minimum. This is a configuration mixing effect that drives the wave function to more deformed, symmetrical shapes, while remaining soft along the γ direction. The 2_1^+ and 4_1^+ states (not shown) exhibit very similar wave functions to the ground state one. These results agree with the experimental findings of a ground state with an average γ close to maximum triaxiality and the increased collectivity in the 4^+ yrast state. The wave function of the 2_2^+ state, the head of the γ-band in our calculation, is shown in panel d). Its maximum is at $\gamma = 30°$ and it has the same β value as the ground state and is also soft in γ. Lastly, in panel c) the wave function of the 0_2^+ state is displayed. It represents a well-defined configuration peaking at $\beta \approx 0.45$, $\gamma \approx 20°$ and contains

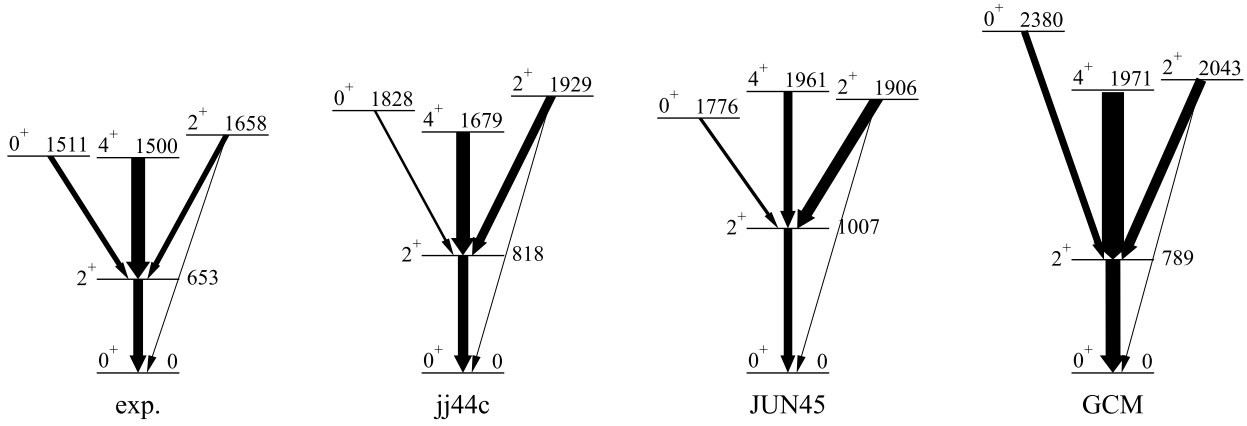

Fig. 4. A comparison of the experimental ^{72}Zn level scheme to shell-model calculations in the jj44 model space (see text for details) using the jj44c [34,35] and JUN45 effective interactions [36]. The results of the beyond mean field GCM calculations are shown on the right. The width of the arrows represent the reduced $E2$ transition strengths.

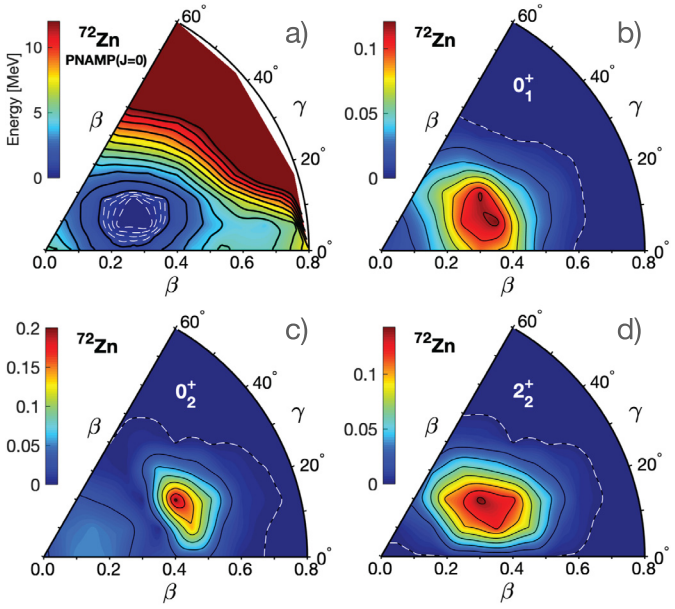

Fig. 5. Panel a): Potential energy surface in the PNAMP approach. The energy minimum has been set to zero. The black contour lines start at 1 MeV and increase in steps of 1 MeV. The white dotted contours start at 0.2 MeV and increase by 0.2 MeV up to 0.8 MeV. Panels b), c) and d): Collective wave functions of the ground, the 0_2^+, and the 2_2^+ states, respectively. The latter is the predicted head of the γ-band. The eight contours start at 0.2 (white dotted line) and increase in steps of 0.2. In Ref. [12] similar calculations were performed for the ground state of ^{72}Zn with a less dense grid of (β, γ) points.

small admixtures of nearly spherical shapes. The main component of this wave function, at variance with the other states, corresponds to a configuration with six particles in the $\nu 0g_{9/2}$ orbital.

In conclusion, the transitional nucleus ^{72}Zn has been studied by multiple Coulomb excitation. The high angular coverage of C-REX allowed extraction of electromagnetic matrix elements. The $B(E2)$ value for the $2_1^+ \rightarrow 0_1^+$ transition agrees with previous measurements, while the $4_1^+ \rightarrow 2_1^+$ transition is more collective than previous lifetime measurements suggested. Quadrupole invariants extracted from the data show that the ground state of ^{72}Zn is moderately deformed and with an average γ close to maximum triaxiality, in agreement with beyond mean-field GCM and the shell-model calculations. The quadrupole moments of the first and second 2^+ states have different signs indicating different deformation. The shell-model calculations indicate that the structure of the excited 0_2^+ state is of a more spherical nature, indicated by increased shell-model configurations with two neutrons occupying the $0g_{9/2}$ orbital. This is in contrast to the GCM results where the 0_2^+ state is more deformed and rigid triaxial. Overall, our results place the ^{72}Zn nucleus between the spherical ^{68}Ni at the $N = 40$ sub-shell closure and the (rigid) triaxial deformed Ge isotopes. Our findings also indicate the presence of distinct configurations with different shapes in ^{72}Zn at low excitation energies.

We want to thank the ISOLDE accelerator group as well as the RILIS team providing us with an excellent pure and highly intense ^{72}Zn beam. We would like to thank B.A. Brown for providing us with the interaction input file and for stimulating discussions. This work was supported by the German BMBF under grant numbers (05P12 WOFNF, 05P12PKFNE), by the DFG (EXC 153) and by ENSAR. D.M. acknowledges the support from NSERC. K.W. acknowledges the support from the Spanish Ministerio de Economía y Competitividad RYC-2017-22007. M.S. acknowledges support from the UK-STFC (grant ST/P005101/1).

Declaration of competing interest

The authors declare that they have no known competing financial interests or personal relationships that could have appeared to influence the work reported in this paper.

Data availability

Data will be made available on request.

References

[1] A. Bohr, Dan. Mat.-Fys. Medd. 26 (1952) 14.
[2] A. Davydov, G. Filippov, Nucl. Phys. 8 (1958) 237, https://doi.org/10.1016/0029-5582(58)90153-6, http://www.sciencedirect.com/science/article/pii/0029558258901536.
[3] L. Wilets, M. Jean, Phys. Rev. 102 (1956) 788, https://doi.org/10.1103/PhysRev.102.788, https://link.aps.org/doi/10.1103/PhysRev.102.788.
[4] B. Kotliński, T. Czosnyka, D. Cline, J. Srebrny, C. Wu, A. Bäcklin, L. Hasselgren, L. Westerberg, C. Baktash, S. Steadman, Nucl. Phys. A 519 (1990) 646, https://doi.org/10.1016/0375-9474(90)90451-Q, http://www.sciencedirect.com/science/article/pii/037594749090451Q.
[5] Y. Toh, C.J. Chiara, E.A. McCutchan, W.B. Walters, R.V.F. Janssens, M.P. Carpenter, S. Zhu, R. Broda, B. Fornal, B.P. Kay, F.G. Kondev, W. Królas, T. Lauritsen, C.J. Lister, T. Pawłat, D. Seweryniak, I. Stefanescu, N.J. Stone, J. Wrzesiński, K. Higashiyama, N. Yoshinaga, Phys. Rev. C 87 (2013) 041304, https://doi.org/10.1103/PhysRevC.87.041304, https://link.aps.org/doi/10.1103/PhysRevC.87.041304.
[6] A.D. Ayangeakaa, R.V.F. Janssens, S. Zhu, D. Little, J. Henderson, C.Y. Wu, D.J. Hartley, M. Albers, K. Auranen, B. Bucher, M.P. Carpenter, P. Chowdhury, D. Cline, H.L. Crawford, P. Fallon, A.M. Forney, A. Gade, A.B. Hayes, F.G. Kondev Krishichayan, T. Lauritsen, J. Li, A.O. Macchiavelli, D. Rhodes, D. Seweryniak, S.M.

Stolze, W.B. Walters, J. Wu, Phys. Rev. Lett. 123 (2019) 102501, https://doi.org/10.1103/PhysRevLett.123.102501, https://link.aps.org/doi/10.1103/PhysRevLett.123.102501.

[7] S. Leenhardt, O. Sorlin, M. Porquet, F. Azaiez, J. Angélique, M. Belleguic, C. Borcea, C. Bourgeois, J. Daugas, C. Donzaud, I. Deloncle, J. Duprat, A. Gillibert, S. Grévy, D. Guillemaud-Mueller, J. Kiener, M. Lewitowicz, S. Lukyanov, F. Marie, N. Orr, Y.-E. Penionzhkevich, F. de Oliveira Santos, F. Pougheon, M. Saint-Laurent, W. Shuying, Y. Sobolev, J. Winfield, Eur. Phys. J. A 14 (2002), https://link.springer.com/article/10.1140%2Fepja%2Fiepja1358.

[8] J. Van de Walle, F. Aksouh, T. Behrens, V. Bildstein, A. Blazhev, J. Cederkäll, E. Clément, T.E. Cocolios, T. Davinson, P. Delahaye, J. Eberth, A. Ekström, D.V. Fedorov, V.N. Fedosseev, L.M. Fraile, S. Franchoo, R. Gernhauser, G. Georgiev, D. Habs, K. Heyde, G. Huber, M. Huyse, F. Ibrahim, O. Ivanov, J. Iwanicki, J. Jolie, O. Kester, U. Köster, T. Kröll, R. Krücken, M. Lauer, A.F. Lisetskiy, R. Lutter, B.A. Marsh, P. Mayet, O. Niedermaier, M. Pantea, R. Raabe, P. Reiter, M. Sawicka, H. Scheit, G. Schrieder, D. Schwalm, M.D. Seliverstov, T. Sieber, G. Sletten, N. Smirnova, M. Stanoiu, I. Stefanescu, J.-C. Thomas, J.J. Valiente-Dobón, P.V. Duppen, D. Verney, D. Voulot, N. Warr, D. Weisshaar, F. Wenander, B.H. Wolf, M. Zielińska, Phys. Rev. C 79 (2009) 014309, https://link.aps.org/doi/10.1103/PhysRevC.79.014309.

[9] M. Niikura, B. Mouginot, S. Franchoo, I. Matea, I. Stefan, D. Verney, F. Azaiez, M. Assie, P. Bednarczyk, C. Borcea, A. Burger, G. Burgunder, A. Buta, L. Cáceres, E. Clément, L. Coquard, G. de Angelis, G. de France, F. de Oliveira Santos, A. Dewald, A. Dijon, Z. Dombradi, E. Fiori, C. Fransen, G. Friessner, L. Gaudefroy, G. Georgiev, S. Grévy, M. Hackstein, M.N. Harakeh, F. Ibrahim, O. Kamalou, M. Kmiecik, R. Lozeva, A. Maj, C. Mihai, O. Möller, S. Myalski, F. Negoita, D. Pantelica, L. Perrot, T. Pissulla, F. Rotaru, W. Rother, J.A. Scarpaci, C. Stodel, J.C. Thomas, P. Ujic, Phys. Rev. C 85 (2012) 054321, https://link.aps.org/doi/10.1103/PhysRevC.85.054321.

[10] C. Louchart, A. Obertelli, A. Görgen, W. Korten, D. Bazzacco, B. Birkenbach, B. Bruyneel, E. Clément, P.J. Coleman-Smith, L. Corradi, D. Curien, G. de Angelis, G. de France, J.-P. Delaroche, A. Dewald, F. Didierjean, M. Doncel, G. Duchêne, J. Eberth, M.N. Erduran, E. Farnea, C. Finck, E. Fioretto, C. Fransen, A. Gadea, M. Girod, A. Gottardo, J. Grebosz, T. Habermann, M. Hackstein, T. Huyuk, J. Jolie, D. Judson, A. Jungclaus, N. Karkour, S. Klupp, R. Krücken, A. Kusoglu, S.M. Lenzi, J. Libert, J. Ljungvall, S. Lunardi, G. Maron, R. Menegazzo, D. Mengoni, C. Michelagnoli, B. Million, P. Molini, O. Möller, G. Montagnoli, D. Montanari, D.R. Napoli, R. Orlandi, G. Pollarolo, A. Prieto, A. Pullia, B. Quintana, F. Recchia, P. Reiter, D. Rosso, W. Rother, E. Sahin, M.-D. Salsac, F. Scarlassara, M. Schlarb, S. Siem, P.P. Singh, P.-A. Söderström, A.M. Stefanini, O. Stézowski, B. Sulignano, S. Szilner, C. Theisen, C.A. Ur, J.J. Valiente-Dobón, M. Zielinska, Phys. Rev. C 87 (2013) 054302, https://link.aps.org/doi/10.1103/PhysRevC.87.054302.

[11] I. Čeliković, A. Dijon, E. Clément, G. De France, P. Van Isacker, J. Ljungvall, C. Franzen, G. Georgiev, A. Görgen, A. Gottardo, M. Hackstein, T. Hagen, C. Louchart, P. Napiorkowski, A. Obertelli, F. Recchia, W. Rother, S. Siem, B. Sulignano, P. Ujić, J. Valiente-Dobón, M. Zielińska, Acta Phys. Pol. B 44 (2013) 375, https://www.actaphys.uj.edu.pl/fulltext?series=Reg&vol=44&page=375.

[12] A. Illana, A. Jungclaus, R. Orlandi, A. Perea, C. Bauer, J.A. Briz, J.L. Egido, R. Gernhäuser, J. Leske, D. Mücher, J. Pakarinen, N. Pietralla, M. Rajabali, T.R. Rodríguez, D. Seiler, C. Stahl, D. Voulot, F. Wenander, A. Blazhev, H. De Witte, P. Reiter, M. Seidlitz, B. Siebeck, M.J. Vermeulen, N. Warr, Phys. Rev. C 89 (2014) 054316, https://doi.org/10.1103/PhysRevC.89.054316, https://link.aps.org/doi/10.1103/PhysRevC.89.054316.

[13] X.F. Yang, Y. Tsunoda, C. Babcock, J. Billowes, M.L. Bissell, K. Blaum, B. Cheal, K.T. Flanagan, R.F. Garcia Ruiz, W. Gins, C. Gorges, L.K. Grob, H. Heylen, S. Kaufmann, M. Kowalska, J. Krämer, S. Malbrunot-Ettenauer, R. Neugart, G. Neyens, W. Nörtershäuser, T. Otsuka, J. Papuga, R. Sánchez, C. Wraith, L. Xie, D.T. Yordanov, Phys. Rev. C 97 (2018) 044324, https://doi.org/10.1103/PhysRevC.97.044324, https://link.aps.org/doi/10.1103/PhysRevC.97.044324.

[14] T.R. Rodríguez, J.L. Egido, Phys. Rev. C 81 (2010) 064323, https://doi.org/10.1103/PhysRevC.81.064323, https://link.aps.org/doi/10.1103/PhysRevC.81.064323.

[15] J.P. Delaroche, M. Girod, J. Libert, H. Goutte, S. Hilaire, S. Péru, N. Pillet, G.F. Bertsch, Phys. Rev. C 81 (2010) 014303, https://doi.org/10.1103/PhysRevC.81.014303, https://link.aps.org/doi/10.1103/PhysRevC.81.014303.

[16] M. Rocchini, K. Hadyńska-Klęk, A. Nannini, A. Goasduff, M. Zielińska, D. Testov, T.R. Rodríguez, A. Gargano, F. Nowacki, G. De Gregorio, H. Naïdja, P. Sona, J.J. Valiente-Dobón, D. Mengoni, P.R. John, D. Bazzacco, G. Benzoni, A. Boso, P. Cocconi, M. Chiari, D.T. Doherty, F. Galtarossa, G. Jaworski, M. Komorowska, N. Marchini, M. Matejska-Minda, B. Melon, R. Menegazzo, P.J. Napiorkowski, D. Napoli, M. Ottanelli, A. Perego, L. Ramina, M. Rampazzo, F. Recchia, S. Riccetto, D. Rosso, M. Siciliano, Onset of triaxial deformation in ^{66}Zn and properties of its first excited 0^+ state studied by means of Coulomb excitation, Phys. Rev. C 103 (2021) 014311, https://doi.org/10.1103/PhysRevC.103.014311, https://link.aps.org/doi/10.1103/PhysRevC.103.014311.

[17] K. Heyde, J.L. Wood, Shape coexistence in atomic nuclei, Rev. Mod. Phys. 83 (2011) 1467–1521, https://doi.org/10.1103/RevModPhys.83.1467, https://link.aps.org/doi/10.1103/RevModPhys.83.1467.

[18] Y. Tsunoda, T. Otsuka, N. Shimizu, M. Honma, Y. Utsuno, Phys. Rev. C 89 (2014) 031301, https://doi.org/10.1103/PhysRevC.89.031301, https://link.aps.org/doi/10.1103/PhysRevC.89.031301.

[19] C.J. Prokop, B.P. Crider, S.N. Liddick, A.D. Ayangeakaa, M.P. Carpenter, J.J. Carroll, J. Chen, C.J. Chiara, H.M. David, A.C. Dombos, S. Go, J. Harker, R.V.F. Janssens, N. Larson, T. Lauritsen, R. Lewis, S.J. Quinn, F. Recchia, D. Seweryniak, A. Spyrou, S. Suchyta, W.B. Walters, S. Zhu, Phys. Rev. C 92 (2015) 061302, https://doi.org/10.1103/PhysRevC.92.061302, https://link.aps.org/doi/10.1103/PhysRevC.92.061302.

[20] P. Van Duppen, K. Riisager, J. Phys. G 38 (2011) 024005, https://doi.org/10.1088/0954-3899/38/2/024005.

[21] P. Reiter, N. Warr, Prog. Part. Nucl. Phys. 113 (2020) 103767, http://www.sciencedirect.com/science/article/pii/S0146641020300144.

[22] V. Fedosseev, K. Chrysalidis, T. Day Goodacre, B. Marsh, S. Rothe, C. Seiffert, K. Wendt, J. Phys. G 44 (2017) 084006, https://doi.org/10.1088/1361-6471/aa78e0.

[23] S.C. Hellgartner, Probing Nuclear Shell Structure beyond the $N = 40$ Subshell using Multiple Coulomb Excitation and Transfer Experiments, Ph.D. thesis, Technische Universität München, Lehrstuhl E12 für Experimentalphysik, 2015, https://mediatum.ub.tum.de/node?id=1277804.

[24] N. Warr, J. Van de Walle, M. Albers, F. Ames, B. Bastin, C. Bauer, V. Bildstein, A. Blazhev, S. Bönig, N. Bree, B. Bruyneel, P. Butler, J. Cederkäll, E. Clément, T. Cocolios, T. Davinson, H. De Witte, P. Delahaye, D. DiJulio, J. Diriken, J. Eberth, A. Ekström, J. Elseviers, S. Emhofer, D. Fedorov, V. Fedosseev, S. Franchoo, C. Fransen, L. Gaffney, J. Gerl, G. Georgiev, R. Gernhäuser, T. Grahn, D. Habs, H. Hess, A. Hurst, M. Huyse, O. Ivanov, J. Iwanicki, D. Jenkins, J. Jolie, N. Kesteloot, O. Kester, U. Köster, M. Krauth, T. Kröll, R. Krücken, M. Lauer, J. Leske, K. Lieb, R. Lutter, L. Maier, B. Marsh, D. Mücher, M. Münch, O. Niedermaier, J. Pakarinen, M. Pantea, G. Pascovici, N. Patronis, D. Pauwels, A. Petts, N. Pietralla, R. Raabe, E. Rapisarda, P. Reiter, A. Richter, O. Schaile, M. Scheck, H. Scheit, G. Schrieder, D. Schwalm, M. Seidlitz, M. Seliverstov, T. Sieber, H. Simon, K.-H. Speidel, C. Stahl, I. Stefanescu, P. Thirolf, H.-G. Thomas, M. Thürauf, P. Van Duppen, D. Voulot, R. Wadsworth, G. Walter, D. Weißhaar, F. Wenander, A. Wiens, K. Wimmer, B. Wolf, P. Woods, K. Wrzosek-Lipska, K. Zell, Eur. Phys. J. A 49 (2013) 40, https://doi.org/10.1140/epja/i2013-13040-9.

[25] Vinzenz Bildstein, Roman Gernhäuser, Thorsten Kröll, Reiner Krücken, Kathrin Wimmer, Piet Van Duppen, Mark Huyse, Nikolas Patronis, Riccardo Raabe, T-REX Collaboration, Eur. Phys. J. A 48 (2012) 85, https://doi.org/10.1140/epja/i2012-12085-6.

[26] K. Alder, A. Winther, Phys. Rev. 91 (1953) 1578.

[27] H. Ower, The Coulex code CLX/DCY, unpublished.

[28] A. Winther, J. de Boer, Academic Press, New York / London, 1966.

[29] D. Cline, T. Czosnyka, A. Hayes, P. Napiorkowski, N. Warr, C. Wu, GOSIA user manual for simulation and analysis of Coulomb excitation experiments, http://www.pas.rochester.edu/~cline/Gosia/Gosia_Manual_20120510.pdf, 2012.

[30] M. Zielińska, L.P. Gaffney, K. Wrzosek-Lipska, E. Clément, T. Grahn, N. Kesteloot, P. Napiorkowski, J. Pakarinen, P.V. Duppen, N. Warr, Eur. Phys. J. A 52 (2016) 99.

[31] B. Pritychenko, M. Birch, B. Singh, M. Horoi, At. Data Nucl. Data Tables 107 (2016) 1, https://doi.org/10.1016/j.adt.2015.10.001, http://www.sciencedirect.com/science/article/pii/S0092640X15000406.

[32] Evaluated nuclear structure data file, https://www.nndc.bnl.gov/ensdf/, 2020.

[33] D. Mücher, G. Gürdal, K.-H. Speidel, G.J. Kumbartzki, N. Benczer-Koller, S.J.Q. Robinson, Y.Y. Sharon, L. Zamick, A.F. Lisetskiy, R.J. Casperson, A. Heinz, B. Krieger, J. Leske, P. Maier-Komor, V. Werner, E. Williams, R. Winkler, Phys. Rev. C 79 (2009) 054310, https://link.aps.org/doi/10.1103/PhysRevC.79.054310.

[34] S. Mukhopadhyay, B.P. Crider, B.A. Brown, S.F. Ashley, A. Chakraborty, A. Kumar, M.T. McEllistrem, E.E. Peters, F.M. Prados-Estévez, S.W. Yates, Nuclear structure of ^{76}Ge from inelastic neutron scattering measurements and shell model calculations, Phys. Rev. C 95 (2017) 014327, https://doi.org/10.1103/PhysRevC.95.014327, https://link.aps.org/doi/10.1103/PhysRevC.95.014327.

[35] B.A. Brown, Priv. comm., 2020.

[36] M. Honma, T. Otsuka, T. Mizusaki, M. Hjorth-Jensen, Phys. Rev. C 80 (2009), https://journals.aps.org/prc/abstract/10.1103/PhysRevC.80.064323.

[37] M. Doncel, A. Gadea, J.J. Valiente-Dobón, B. Quintana, V. Modamio, D. Mengoni, O. Möller, A. Dewald, N. Pietralla, Determination of lifetimes of nuclear excited states using the recoil distance Doppler shift method in combination with magnetic spectrometers, Eur. Phys. J. A 53 (2017) 211, https://doi.org/10.1140/epja/i2017-12382-6.

[38] N. Shimizu, T. Mizusaki, Y. Utsuno, Y. Tsunoda, Thick-restart block Lanczos method for large-scale shell-model calculations, Comput. Phys. Commun. 244 (2019) 372, https://doi.org/10.1016/j.cpc.2019.06.011, http://www.sciencedirect.com/science/article/pii/S0010465519301985.

[39] B. Cheal, E. Mané, J. Billowes, M.L. Bissell, K. Blaum, B.A. Brown, F.C. Charlwood, K.T. Flanagan, D.H. Forest, C. Geppert, M. Honma, A. Jokinen, M. Kowalska, A. Krieger, J. Krämer, I.D. Moore, R. Neugart, G. Neyens, W. Nörtershäuser, M. Schug, H.H. Stroke, P. Vingerhoets, D.T. Yordanov, M. Žáková, Phys. Rev. Lett. 104 (2010) 252502, https://doi.org/10.1103/PhysRevLett.104.252502, https://link.aps.org/doi/10.1103/PhysRevLett.104.252502.

[40] O. Sorlin, S. Leenhardt, C. Donzaud, J. Duprat, F. Azaiez, F. Nowacki, H. Grawe, Z. Dombrádi, F. Amorini, A. Astier, D. Baiborodin, M. Belleguic, C. Borcea, C. Bourgeois, D.M. Cullen, Z. Dlouhy, E. Dragulescu, M. Górska, S. Grévy, D. Guillemaud-Mueller, G. Hagemann, B. Herskind, J. Kiener, R. Lemmon, M. Lewitowicz, S.M. Lukyanov, P. Mayet, F. de Oliveira Santos, D. Pantalica, Y.-E. Penionzhkevich, F.

Pougheon, A. Poves, N. Redon, M.G. Saint-Laurent, J.A. Scarpaci, G. Sletten, M. Stanoiu, O. Tarasov, C. Theisen, $^{68}_{28}Ni_{40}$: magicity versus superfluidity, Phys. Rev. Lett. 88 (2002) 092501, https://doi.org/10.1103/PhysRevLett.88.092501, https://link.aps.org/doi/10.1103/PhysRevLett.88.092501.

[41] K. Langanke, J. Terasaki, F. Nowacki, D.J. Dean, W. Nazarewicz, How magic is the magic ^{68}Ni nucleus?, Phys. Rev. C 67 (2003) 044314, https://doi.org/10.1103/PhysRevC.67.044314, https://link.aps.org/doi/10.1103/PhysRevC.67.044314.

[42] K. Kumar, Phys. Rev. Lett. 28 (1972) 249, https://doi.org/10.1103/PhysRevLett.28.249, https://link.aps.org/doi/10.1103/PhysRevLett.28.249.

[43] D. Cline, Annu. Rev. Nucl. Part. Sci. 36 (1986) 683, https://doi.org/10.1146/annurev.ns.36.120186.003343.

[44] J. Henderson, Phys. Rev. C 102 (2020) 054306, https://doi.org/10.1103/PhysRevC.102.054306, https://link.aps.org/doi/10.1103/PhysRevC.102.054306.